Acta Crystallographica Section B
**Structural Science, Crystal Engineering and Materials**
ISSN 2052-5206

# Prediction of possible $CaMnO_3$ modifications using an *ab initio* minimization data-mining approach

**Jelena Zagorac,[a]* Dejan Zagorac,[a,b] Aleksandra Zarubica,[c] J. Christian Schön,[b] Katarina Djuris[b] and Branko Matovic[a]**

[a]Materials Science Laboratory, Institute of Nuclear Sciences Vinča, Belgrade University, PO Box 522, 11001 Belgrade, Serbia, [b]Max Planck Institute for Solid State Research, Heisenbergstr. 1, 70569 Stuttgart, Germany, and [c]Department of Chemistry, University of Niš, Višegradska 33, 18000 Niš, Serbia

Correspondence e-mail: jelena@vin.bg.ac.rs

Received 29 January 2014
Accepted 5 June 2014

We have performed a crystal structure prediction study of $CaMnO_3$ focusing on structures generated by octahedral tilting according to group–subgroup relations from the ideal perovskite type ($Pm\bar{3}m$), which is the aristotype of the experimentally known $CaMnO_3$ compound in the *Pnma* space group. Furthermore, additional structure candidates have been obtained using data mining. For each of the structure candidates, a local optimization on the *ab initio* level using density-functional theory (LDA, hybrid B3LYP) and the Hartree–Fock (HF) method was performed, and we find that several of the modifications may be experimentally accessible. In the high-pressure regime, we identify a post-perovskite phase in the $CaIrO_3$ type, not previously observed in $CaMnO_3$. Similarly, calculations at effective negative pressure predict a phase transition from the orthorhombic perovskite to an ilmenite-type ($FeTiO_3$) modification of $CaMnO_3$.

## 1. Introduction

$CaMnO_3$-based ceramics have many industrial applications, because of their good electrical conductivity and magnetic properties (Vecherskii *et al.*, 2002; Raveau *et al.*, 1998). Their physical properties are intimately related to their crystal structure, which exhibit the perovskite structure-type. Since $CaMnO_3$ is an important industrial material, it is of great interest to identify possible new stable and metastable modifications and investigate their structural relationships. The perovskite family of structures with $ABX_3$ stoichiometry is known as one of the most frequent structure types in the field of mineralogy and material science, since it accommodates most of the metallic ions at both *A* and *B* cation sites, and a number of different anions at the *X*-positions (Mitchell, 2002; Coey *et al.*, 1999). The symmetry of an ideal perovskite is $Pm\bar{3}m$, but it is commonly reduced from the cubic to a lower symmetry due to the substitution of cations of different size at the *A* and *B* sites. Frequently, metastable structures between the maximally symmetric ($Pm\bar{3}m$) and the equilibrium structure exist over a limited temperature and/or pressure range, for the given cations.

Octahedral tilting is the most common type of distortion in the perovskite structure type (Woodward, 1997), where the actual tilt system depends largely on the temperature, pressure and composition. It is known that the octahedral tilting reduces the symmetry at the *A*-site cation and leads to a change in the *A*—O bond lengths (Brown, 1992). The octahedra can tilt in different ways, each resulting in a different coordination environment for the *A*-site cation (Glazer, 1972).

© 2014 International Union of Crystallography

In his study, Glazer describes only tilts where just two successive layers are involved. An alternative, equally valid notation of octahedra tilting has been developed by Aleksandrov (1976). A group-theoretical analysis of simple tilt systems has been performed by Howard & Stokes (1998). According to this approach, 15 possible tilt systems can occur in $ABX_3$ perovskites, each with a unique space group (Fig. 1). Besides the effect on the crystal structure, the existence and magnitude of an octahedral tilting distortion also have a large influence on a great number of physical properties (Hwang *et al.*, 1995; Mitchell & Liferovich, 2005; Colla *et al.*, 1993).

Thus, there has been an enormous scientific interest in perovskites in the last decades, both experimentally and theoretically (Evarestov *et al.*, 2011; Maier *et al.*, 2011; Ederer & Spaldin, 2006; Oganov *et al.*, 2005; Zhao *et al.*, 2004; Tong *et al.*, 2010; Locherer *et al.*, 2012). The relative stability of the various modifications of the perovskite structure type has been investigated theoretically in the past; examples are simple geometric considerations based on the ionic radii (Goldschmidt, 1926), a bond-valence analysis (Brown & Altermatt, 1985) that is also employed in the SPuDS (Structure Prediction Diagnostic Software; Lufaso & Woodward, 2001) and *ab initio* calculations (Caracas & Wentzcovitch, 2006; Magyari-Köpe *et al.*, 2001; Wentzcovitch *et al.*, 1995).

Specifically with regard to $CaMnO_3$, there have been many experimental investigations of $CaMnO_3$ (Poeppelmeier *et al.*, 1982; Taguchi, 1996; Božin *et al.*, 2008; Zagorac *et al.*, 2010; Zhou & Kennedy, 2006) and several theoretical calculations (Paszkowicz *et al.*, 2013; Freyria Fava *et al.*, 1997; Trang *et al.*, 2011). *Ab initio* calculations are usually most reliable yet typically non-trivial and time consuming, especially if one employs several theoretical approaches (Avdeev *et al.*, 2007). Since phase diagrams do not exist for most of the compounds with the perovskite structure type this would be a valuable contribution to the systematic investigations of the structure(s) of $CaMnO_3$ with respect to the pressure and temperature (Magyari-Köpe *et al.*, 2001; Thomas, 1998).

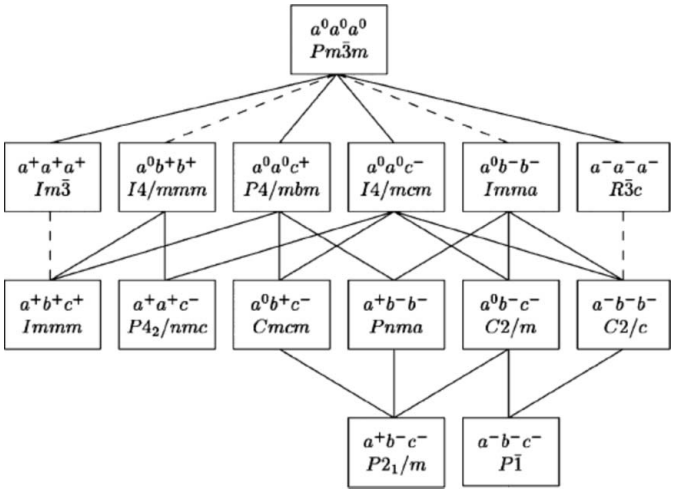


**Figure 1**
Group–subgroup relation graph for $ABX_3$ perovskites (reproduced from Howard & Stokes, 1998). Solid and dashed lines join group–subgroup pairs and could correspond to phase transitions of second and first order, respectively. Note that the tilt systems are indicated above the space groups.

Our starting point was the group–subgroup relation graph (Fig. 1; Howard & Stokes, 1998) starting from the ideal cubic perovskite structure (space group $Pm\bar{3}m$), to the final low symmetry $P2_1/m$ and $P\bar{1}$ space groups, where the effects of octahedral tilting and general distortions of the ideal perovskite structure are most pronounced. The main goal of this research was to investigate possible perovskite-type modifications and group–subgroup relations of the $CaMnO_3$ compound.

Using the SPuDS software, we have investigated the applicability of the bond-valence approach in conjunction with *ab initio* total energy calculations in the prediction of the possible phase transitions in the $CaMnO_3$ perovskite. In addition, the search for new crystalline structures in $CaMnO_3$ was extended *via* data mining to low and high-pressure modifications, where the latter are often denoted as 'post-perovskite' structure types.

## 2. Computational details

In this study we have combined two search methods in order to generate new structure candidates for $CaMnO_3$, followed by local optimizations on the *ab initio* level (Zagorac *et al.*, 2013). In the first step of the search, we have used the Structure Prediction Diagnostic Software (SPuDS; Lufaso & Woodward, 2001) to produce new structure candidates of $CaMnO_3$ perovskites. The SPuDS program was developed to predict the crystal structures of perovskites, including those distorted by tilting of symmetric and Jahn–Teller distorted octahedra (Lufaso & Woodward, 2004). The stability of the perovskite structure is determined by comparing the calculated bond-valence sums and the ideal formal valences. This quantity is known as the global instability index (GII) and it is calculated according to composition in 11 different Glazer tilt systems for a single *B*-site cation (Salinas-Sanchez *et al.*, 1992).

In the next step we have used data mining of the Inorganic Crystal Structure Database (ICSD; Bergerhoff & Brown, 1987) to find additional structure candidates with the general formula $ABX_3$. Afterwards we used *ab initio* energy calculations and minimizations to refine the structure candidates and check which of the candidates are kinetically stable and how they should be ranked in energy, as a function of pressure and temperature.

The full geometry optimization is performed using the *CRYSTAL09* code, which is based on local GAUSSIAN-type orbitals (Dovesi *et al.*, 2005). For the *ab initio* calculations an all-electron basis set (AEBS) for Ca, Mn and O were used as given in Freyria Fava *et al.* (1997) and shown in the supporting information (Table S1[1]). In the case of $Ca^{2+}$ a [5*s*4*p*1*d*] basis set (*i.e.* consisting of five *s*, four *p* and one *d* functions) was

[1] Supporting information for this paper is available from the IUCr electronic archives (Reference: HW5032).

used. For $Mn^{4+}$ a [5*s*4*p*2*d*] basis set was used, and for $O^{2-}$ a [4*s*3*p*] all-electron basis set was used, respectively.

The local optimizations employed analytical gradients with respect to the atom positions and the cell parameters, and a local optimization routine (Doll *et al.*, 2001). These local optimizations were performed using DFT (LDA, hybrid B3LYP functionals) and the Hartree–Fock approach. It is reasonable to choose at least two different *ab initio* methods, in order to gain better insight in the quantitative validity of the results (Schön *et al.*, 2004; Zagorac *et al.*, 2011, 2014). In each case, we performed the local optimization within the prescribed space group resulting in the $E(V)$ curves. Of course, these distorted configurations are expected to further relax to the experimentally observed low-temperature structure once the symmetry constraints are removed. However, we note that due to the nearby energies of the closely related distorted structures, one can often expect that at medium to elevated temperatures (at low temperature kinetically unstable) the high-symmetry modifications become thermodynamically stable or at least metastable compared with the global minimum structure.

Since it is possible, in principle, that additional symmetries appear during the local optimization, the symmetry of the optimized structures was analyzed with the algorithms SFND ('Symmetry FiNDer'; Hundt *et al.*, 1999) and RGS, meaning 'Raum Gruppen Sucher' (= space group seeker; Hannemann *et al.*, 1998), as implemented in the program *KPLOT* (Hundt, 2012). The structures investigated were visualized using *KPLOT* and *VESTA* (Momma & Izumi, 2011) software.

**Table 1**
Calculated values of the global instability index (GII) for 11 $CaMnO_3$ modifications using SPuDS.

| Name | Space group | Tilt system | GII (a.u.) |
|---|---|---|---|
| $CaMnO_3$-(1) | *Pnma* | $a^-b^+a^-$ | 0.00003 |
| $CaMnO_3$-(2) | $R\bar{3}c$ | $a^-a^-a^-$ | 0.00018 |
| $CaMnO_3$-(3) | *Imma* | $a^0b^-b^-$ | 0.00849 |
| $CaMnO_3$-(4) | $P4_2/nmc$ | $a^+a^+c^-$ | 0.01747 |
| $CaMnO_3$-(5) | *Cmcm* | $a^+b^0c^-$ | 0.01861 |
| $CaMnO_3$-(6) | *P*4/*mbm* | $a^0a^0c^+$ | 0.02220 |
| $CaMnO_3$-(7) | *I*4/*mcm* | $a^0a^0c^-$ | 0.02220 |
| $CaMnO_3$-(8) | $Im\bar{3}$ | $a^+a^+a^+$ | 0.04723 |
| $CaMnO_3$-(9) | *I*4/*mmm* | $a^0b^+b^+$ | 0.05017 |
| $CaMnO_3$-(10) | *C*2/*c* | $a^-b^-b^-$ | 0.06327 |
| $CaMnO_3$-(11) | $Pm\bar{3}m$ | $a^0a^0a^0$ | 0.15775 |

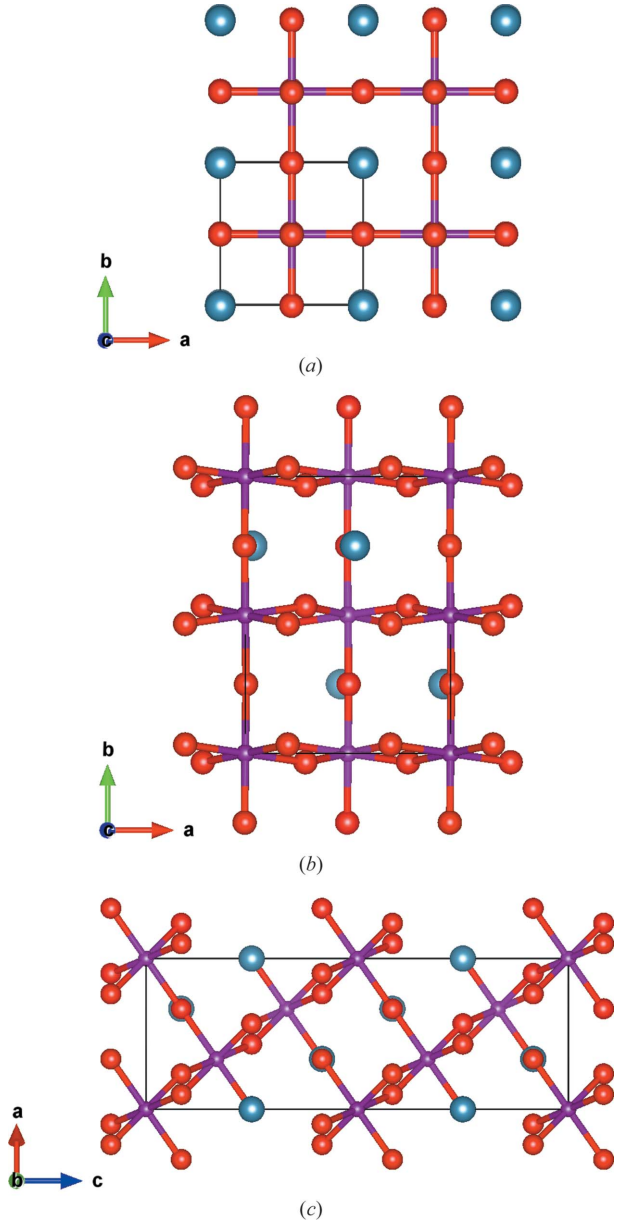


**Figure 2**
Calculated $CaMnO_3$ modifications using the B3LYP approximation: (*a*) $CaMnO_3$-(11) in the space group $Pm\bar{3}m$; (*b*) $CaMnO_3$-(1) in the space group *Pnma*; (*c*) $CaMnO_3$-(2) in the space group $R\bar{3}c$. Mn (violet) and O (red) atoms are bonded, and Ca atoms are colored blue. The unit cell is marked with a quadrangle.

## 3. Results

### 3.1. Structure prediction

Using the SPuDS software, 11 perovskite-related structure candidates $CaMnO_3$-(1 − 11) in different space groups were obtained and sorted according to their GII values (Table 1). Based on the GII criterion, the most stable $CaMnO_3$ perovskite structure is the experimentally observed one $CaMnO_3$-(1) in the space group *Pnma*, with GII = 0.00003 (Table 1). The most unstable structure is the cubic $Pm\bar{3}m$ perovskite $CaMnO_3$-(11) with *GII* = 0.15775. As mentioned before, the distortions away from the ideal perovskite structure occur according to various tilt systems, resulting in a change of symmetry. Subsequently, additional tilt systems in various space groups are generated for this first set of distorted structures, whose stability lie between the experimentally observed orthorhombic *Pnma* and cubic $Pm\bar{3}m$ configurations (*cf.* Table 1). For example, the symmetry of $CaMnO_3$ is lowered from cubic ($Pm\bar{3}m$, $Z = 1$) to orthorhombic (*Pnma*, $Z = 4$) by tilting of the $MnO_6$ octahedra (Figs. 2*a* and *b*). This distortion is driven by the difference in size between the cube-octahedral cavity in the octahedral network and the smaller ionic radius of the $Ca^{2+}$ ion. When the radii of the *A* and *B* site

cations fulfill the requirements of the Goldschmidt tolerance factor, $G_t$ = 1, the perovskite is stable and exhibits a cubic symmetry (Goldschmidt, 1926). With a value of $G_t$ = 0.97, $CaMnO_3$ has an orthorhombic perovskite structure with space group *Pnma* at 298 K and atmospheric pressure (Taguchi, 1996; Božin *et al.*, 2008; Zagorac *et al.*, 2010).

In the next phase, a data-mining method was applied in order to search for additional structure candidates with the general formula $ABX_3$, with a particular focus on structures related to the perovskite family. A summary of all structure candidates is presented in the supporting information (Table S2), where the results of data mining (using the ICSD) can easily be compared to those from the structure prediction using SPuDS.[2] Overall, besides the 11 perovskite structure candidates generated by SPuDS, we have obtained several more related to the perovskite family, $CaMnO_3$-(12,13,14) with space groups *Immm*, *C*2/*m* and *R*3*c*, respectively. In addition, two non-perovskite $ABX_3$ structure types, $CaMnO_3$-(15) (a post-perovskite previously observed in $CaIrO_3$) and $CaMnO_3$-(16) (analogous to ilmenite), were identified.

We note that in the ICSD the $CaMnO_3$ perovskite is listed only in space groups $Pm\bar{3}m$ (theoretically proposed by Trang *et al.*, 2011) and *Pnma* (experimentally determined by Božin *et al.*, 2008, and others). In all other cases the starting perovskite family structural model was taken from other $ABX_3$ compounds, since it is yet unknown theoretically or experimentally in $CaMnO_3$. For example, the starting structural models $CaMnO_3$-(4, 6, 8, 9) were taken from Caracas & Wentzcovitch (2006) where they had been suggested theoretically in the $CaSiO_3$ system (Table S2).

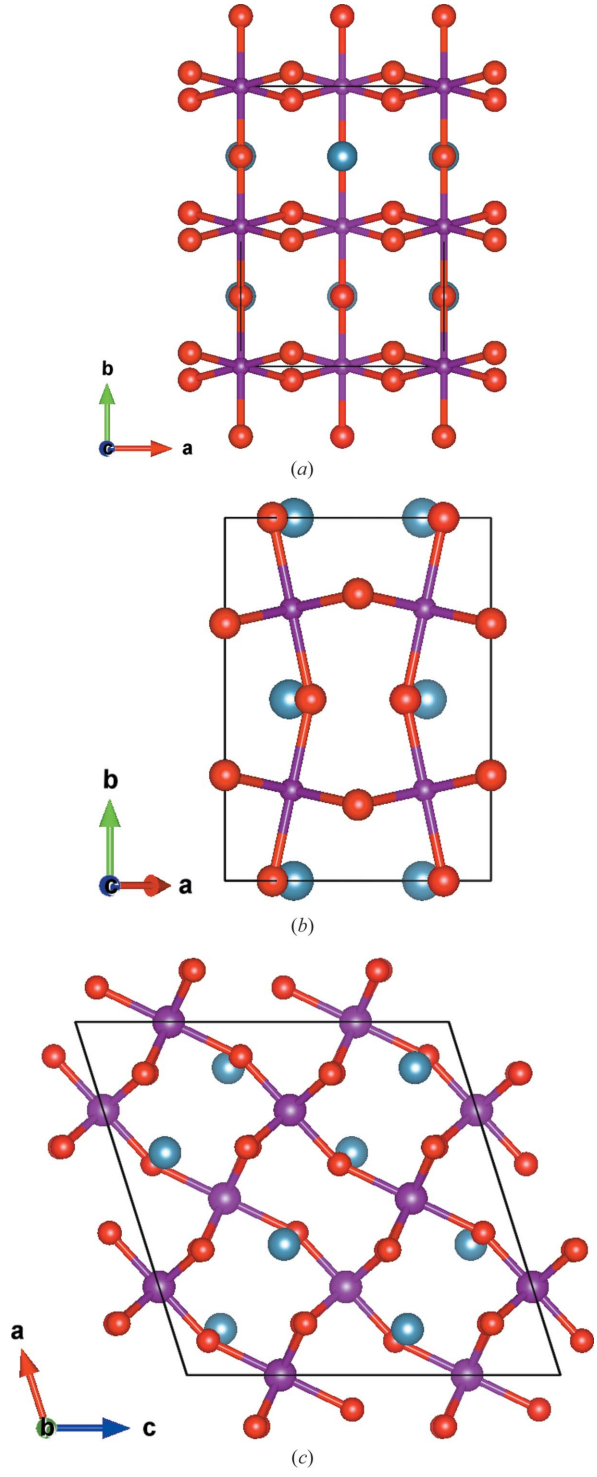


**Figure 3**
Calculated $CaMnO_3$ modifications using the B3LYP approximation: (*a*) $CaMnO_3$-(3) in space group *Imma*; (*b*) $CaMnO_3$-(13) in space group *C*2/*m*; (*c*) $CaMnO_3$-(10) in space group *C*2/*c*. Mn (violet) and O (red) atoms are bonded, and Ca atoms are colored blue. The unit cell is marked with a quadrangle.

### 3.2. Structure optimizations on the *ab initio* level

Next, the structure candidates generated using the procedures described above were submitted to the *ab initio* local optimization. These local optimizations were performed using DFT with both an LDA and a hybrid functional (B3LYP), and the Hartree–Fock (HF) approach, where the space group was kept fixed. A summary of our results is shown in Tables 2, 3 and S3, where the structural parameters and total energies of all optimized structures on *ab initio* level are presented.

When comparing the structural data for the only experimentally observed perovskite structure $CaMnO_3$-(1) (space group *Pnma*; *cf.* Table 2) to our *ab initio* calculations, we see, as expected, that the LDA calculations underestimate the size of the unit cell, while HF overestimates the unit-cell parameters, especially in the *b* direction. In addition, we encounter computational convergence problems when using the Hartree–Fock approach for $CaMnO_3$-(4, 5, 13) (space groups $P4_2/nmc$, *Cmcm* and *C*2/*m*, respectively; see Table 3). In contrast, the B3LYP functional calculations showed good agreement with experiment; this is consistent with earlier comparison studies on perovskite systems (Piskunov *et al.*, 2004; García-Fernández *et al.*, 2012) which also found very good agreement with experiment for hybrid functionals. Furthermore, only for the B3LYP calculations does the configuration with the lowest energy correspond to the experimentally observed one [for LDA, the $CaMnO_3$-(2) $R\bar{3}c$

[2] Of course, there are many more $ABX_3$ structure types in the ICSD (Sultania *et al.*, 2012); however, we have restricted ourselves to those most commonly encountered in compounds that also possess a perovskite-like modification.

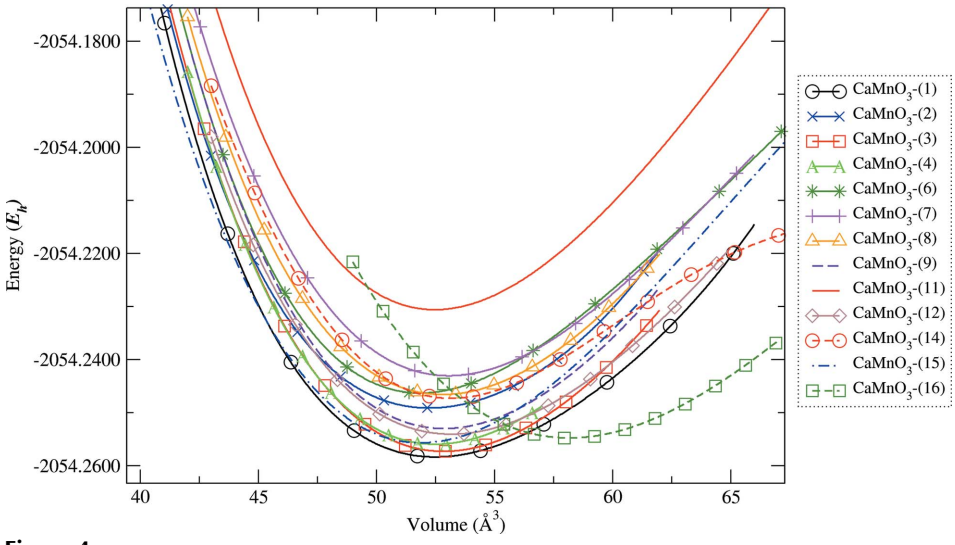


**Figure 4**
$E(V)$ curves at the B3LYP level of calculation for the most relevant modifications of $CaMnO_3$. Energies per formula unit are given in hartrees ($E_h$). Note that the $CaMnO_3$-(5) and $CaMnO_3$-(10) are indistinguishable with respect to calculated energies of $CaMnO_3$-(1), and therefore only the $CaMnO_3$-(1) curve is shown. Similarly, $CaMnO_3$-(4) and $CaMnO_3$-(13) have virtually the same $E(V)$ curve at this scale, and therefore only one curve is shown.

structure, and for HF the $CaMnO_3$-(10) $C2/c$ structure, have the lowest energy, respectively].[3] Thus, in the following only the results obtained using the B3LYP functional are analyzed in more detail.

In the case of the cubic $Pm\bar{3}m$ perovskite $CaMnO_3$-(11) (Fig. 2*a* and Table S3), the unit-cell parameters of 3.75 Å are in excellent agreement with previously reported theoretical studies (Freyria Fava *et al.*, 1997; Bhattacharjee *et al.*, 2009), where $a$ = 3.75 Å. According to the group–subgroup relations (Fig. 1) in the perovskite structure family there are few space groups along the transition path between the aristotype $Pm\bar{3}m$ space group and the *Pnma* space group experimentally found in $CaMnO_3$. We note that the aristotype structure $CaMnO_3$-(11) is the most unstable one in the $CaMnO_3$ system according to the *ab initio* calculation (Table 3) and is furthermore in agreement with the GII-based ranking.

If we now compare the GII (Table 1) and B3LYP results (Table 3) for the other candidate configurations, we observe several differences in the ranking of the candidates. Thus, *e.g.* $CaMnO_3$-(2) (space group $R\bar{3}c$; Fig. 2*c*), which is the second best in the GII table is energetically not so favorable with respect to the *ab initio* B3LYP calculations. The reason for this particular discrepancy is found in the SPuDS software which does not penalize $A$—O and O—O distances that are too short (Brown, 2002), resulting in a GII value that is too low. We also note that $R\bar{3}c$ is a direct subgroup of the cubic $Pm\bar{3}m$ group, for which the $CaMnO_3$ configuration is unstable (see Fig. 1). On the other hand, if we consider the $CaMnO_3$-(3) (space group *Imma*; Fig. 3*a*) perovskite modification its relatively high stability ranking is confirmed from both *GII* and B3LYP calculations. For the monoclinic variants of perovskites $CaMnO_3$-(13) and $CaMnO_3$-(10) in the space groups $C2/m$ (Fig. 3*b*) and $C2/c$ (Fig. 3*c*), respectively, we observe that they are much more favorable on the B3LYP level of calculation than when using the simple GII criterion. Here we also note that *Imma* is a supergroup of both the monoclinic $C2/m$ and $C2/c$ and the experimentally observed *Pnma* (see Fig. 1) space groups.

The energy *versus* volume, $E(V)$, curves were computed for every locally optimized candidate keeping the space group fixed in the process. Fig. 4 shows the $E(V)$ curves computed using the B3LYP functional for the most relevant modifications. The perovskite-related configurations $CaMnO_3$-(3, 13, 10, 4, 12, 9, 5) in the space groups *Imma* (Fig. 3*a*), $C2/m$ (Fig. 3*b*), $C2/c$ (Fig. 3*c*), $P4_2/nmc$ (Fig. S1*a*), *Immm* (Fig. S1*b*) $I4/mmm$ (Fig. S1*c*) and *Cmcm* (Fig. S2*a*), respectively, are nearest to the equilibrium orthorhombic structure. Structure parameters for these favored structures are given in Table 2. Besides the perovskite family structure types, Table 2 contains the post-perovskite ($CaMnO_3$-15) and ilmenite ($CaMnO_3$-16) modifications, since they are thermodynamically stable at elevated and negative pressures, respectively. In contrast, the modifications $CaMnO_3$-(11, 2, 14, 7, 8, 6) in the space groups $Pm\bar{3}m$ (Fig. 2*a*), $R\bar{3}c$ (Fig. 2*c*), $R3c$ (Fig. S2*b*), $I4/mcm$ (Fig. S3*a*), $Im\bar{3}$ (Fig. S3*b*) and $P4/mbm$ (Fig. S3*c*), respectively, are energetically and experimentally unfavorable in the $CaMnO_3$ system (Table S3). In general, we find that the orthorhombic space groups are more favored to occur in the $CaMnO_3$ system than the higher symmetry candidates, which is in agreement with the GII and group–subgroup relation graph criteria (Table 1 and Fig. 1). In this context, we note that quite typically, orthorhombic structures are found for compounds that exhibit the greatest deviation from the ideal cubic structure (Thomas, 1996).

As observed from Table 3 (calculated with the B3LYP functional), other favorable candidates which might be accessible in the experiment are $CaMnO_3$-(10), $CaMnO_3$-(13) and $CaMnO_3$-(4) having space groups $C2/c$, $C2/m$ and tetragonal $P4_2/nmc$. These structures are not so competitive on the LDA level and they are quite unstable on the HF level (see Table 3).[4] Therefore, we consider the $CaMnO_3$-(3) modification in space group *Imma* as an especially good candidate,

[3] Such differences in rankings of slightly distorted structures are frequently encountered and reflect the inherent limitations of the *ab inito* energy calculations.

[4] In addition we note that the $CaMnO_3$-(4) modification has $a > c$ after *ab initio* optimization compared with the starting models (ICSD and SPuDS) where $a < c$ (see Tables 3 and Table S2).

**Table 2**
Structural data of the energetically most favorable $CaMnO_3$ perovskite modifications found after local optimization on LDA, B3LYP, and HF level.

| Modification, space group | Cell parameters (Å), unit-cell volume (Å$^3$) and fractional coordinates | | |
|---|---|---|---|
| and Wyckoff position | LDA | b3lyp | HF |
| $CaMnO_3$-(1) | $a$ = 5.16, $b$ = 7.34, $c$ = 5.14 | $a$ = 5.41, $b$ = 7.30, $c$ = 5.32 | $a$ = 5.40, $b$ = 7.90, $c$ = 5.42 |
| *Pnma* (62) | $V$ = 194.59 | $V$ = 209.76 | $V$ = 230.84 |
| Ca 4*c* | 0.0330 1/4 0.9947 | 0.0339 1/4 0.9919 | 0.0043 1/4 0.9547 |
| Mn 4*b* | 1/2 0 0 | 1/2 0 0 | 1/2 0 0 |
| O1 4*c* | 0.4947 1/4 0.0611 | 0.4967 1/4 0.0597 | 0.4993 1/4 0.1260 |
| O2 8*d* | 0.2884 0.0308 0.7114 | 0.2930 0.0321 0.7147 | 0.2544 0.0530 0.7449 |
| $CaMnO_3$-(3) | $a$ = 5.17, $b$ = 7.26, $c$ = 5.24 | $a$ = 5.35, $b$ = 7.38, $c$ = 5.35 | $a$ = 5.43, $b$ = 6.89, $c$ = 5.44 |
| *Imma* (74) | $V$ = 196.62 | $V$ = 211.37 | $V$ = 203.53 |
| Ca 4*e* | 0 1/4 0.0069 | 0 1/4 0.0116 | 0 1/4 0.0007 |
| Mn 4*b* | 0 0 1/2 | 0 0 1/2 | 0 0 1/2 |
| O1 4*e* | 0 1/4 0.5752 | 0 1/4 0.5781 | 0 1/4 0.5156 |
| O2 8*g* | 1/4 0.9511 3/4 | 1/4 0.9518 3/4 | 1/4 0.9901 3/4 |
| $CaMnO_3$-(4) | $a$ = 7.32, $c$ = 7.28 | $a$ = 7.59, $c$ = 7.30 | † |
| $P4_2/nmc$ (137) | $V$ = 390.04 | $V$ = 420.21 | |
| Ca1 2*a* | 3/4 1/4 3/4 | 3/4 1/4 3/4 | |
| Ca2 2*b* | 3/4 1/4 1/4 | 3/4 1/4 1/4 | |
| Ca3 4*d* | 1/4 1/4 0.2709 | 1/4 1/4 0.2333 | |
| Mn1 8*e* | 0 0 0 | 0 0 0 | |
| O1 8*f* | 0.0287 0.9713 1/4 | 0.0268 0.9732 1/4 | |
| O2 8*g* | 1/4 0.9618 0.0309 | 1/4 0.0411 0.9726 | |
| O3 8*g* | 1/4 0.9660 0.5293 | 1/4 0.9640 0.5325 | |
| $CaMnO_3$-(5) | $a$ = 7.31, $b$ = 7.33, $c$ = 7.34 | $a$ = 7.57, $b$ = 7.56, $c$ = 7.37 | † |
| *Cmcm* | $V$ = 392.76 | $V$ = 421.71 | |
| Ca1 4*c* | 0 0.4886 1/4 | 0 0.4854 1/4 | |
| Ca2 4*c* | 0 0.9875 1/4 | 0 0.9866 1/4 | |
| Mn 8*d* | 1/4 1/4 0 | 1/4 1/4 0 | |
| O 8*e* | 0.2864 0 0 | 0.2881 0 0 | |
| O 8*f* | 0 0.2135 0.0376 | 0 0.2126 0.0413 | |
| O 8*g* | 0.2874 0.2509 1/4 | 0.2855 0.2531 1/4 | |
| $CaMnO_3$-(9) | $a$ = 7.35, $c$ = 7.27 | $a$ = 7.50, $c$ = 7.50 | $a$ = 7.65, $c$ = 7.57 |
| *I*4/*mmm* (139) | $V$ = 392.90 | $V$ = 422.52 | $V$ = 443.06 |
| Ca1 2*a* | 0 0 0 | 0 0 0 | 0 0 0 |
| Ca2 2*b* | 0 0 1/2 | 0 0 1/2 | 0 0 1/2 |
| Ca3 4*c* | 0 1/2 0 | 0 1/2 0 | 0 1/2 0 |
| Mn 8*f* | 1/4 1/4 1/4 | 1/4 1/4 1/4 | 1/4 1/4 1/4 |
| O1 8*h* | 0.2831 0.2831 0 | 0.2856 0.2856 0 | 0.2140 0.2140 0 |
| O2 16*n* | 0 0.2479 0.2855 | 0 0.2474 0.2870 | 0 0.2534 0.2849 |
| $CaMnO_3$-(10) | $a$ = 8.89, $b$ = 5.18, $c$ = 8.83 | $a$ = 9.04, $b$ = 5.39, $c$ = 9.11 | $a$ = 9.07, $b$ = 5.36, $c$ = 9.20 |
| *C*2/*c* (15) | $\beta$ = 107.88, $V$ = 386.92 | $\beta$ = 107.53, $V$ = 422.85 | $\beta$ = 108.13, $V$ = 425.34 |
| Ca 8*f* | 0 8716 0.7506 0.8721 | 0.8704 0.7528 0.8709 | 0.8699 0.7519 0.8706 |
| Mn1 4*e* | 0 0.7497 1/4 | 0 0.7472 1/4 | 0 0.7427 1/4 |
| Mn2 4*d* | 1/4 1/4 1/2 | 1/4 1/4 1/2 | 1/4 1/4 1/2 |
| O1 8*f* | 0.9087 0.7499 0.4077 | 0.9026 0.7471 0.4134 | 0.8925 0.7393 0.4182 |
| O2 8*f* | 0.3524 0.5005 0.6454 | 0 3537 0.5078 0.6395 | 0.3574 0.5080 0.6368 |
| O3 8*f* | 0.1475 0.5001 0.8543 | 0.1452 0.5075 0.8524 | 0.1444 0.5104 0.8542 |
| $CaMnO_3$-(12) | $a$ = 5.13, $b$ = 5.13, $c$ = 7.41 | $a$ = 5.30, $b$ = 5.33, $c$ = 7.50 | $a$ = 5.34, $b$ = 5.24, $c$ = 7.56 |
| *Immm* (71) | $V$ = 194.89 | $V$ = 211.89 | $V$ = 211.67 |
| Ca 4*j* | 1/2 0 0.2498 | 1/2 0 0.2477 | 0 0 0.2478 |
| Mn1 2*a* | 0 0 0 | 0 0 0 | 0 0 0 |
| Mn2 2*c* | 1/2 1/2 0 | 1/2 1/2 0 | 1/2 1/2 0 |
| O1 8*n* | 0.2501 0.2501 1/2 | 0.2567 0.2555 0 | 0.2614 0.2613 0 |
| O2 4*i* | 0 0 0.2501 | 0 0 0.2496 | 0 0 0.2561 |
| $CaMnO_3$-(13) | $a$ = 7.35, $b$ = 7.27, $c$ = 5.17 | $a$ = 7.58, $b$ = 7.32, $c$ = 5.36 | † |
| *C2/m* (12) | $\beta$ = 134.60, $V$ = 196.60 | $\beta$ = 134.98, $V$ = 210.43 | |
| Ca 4*i* | 0.2440 0 0.4942 | 0.2412 0 0.4911 | |
| Mn 4*e* | 1/4 1/4 0 | 1/4 1/4 0 | |
| O1 4*h* | 0 0.2135 1/2 | 0 0.2907 1/2 | |
| O2 4*g* | 0 0.7862 0 | 0 0.7092 0 | |
| O3 4*i* | 0.3184 0 0.0681 | 0.3215 0 0.0717 | |

since it is energetically different enough from the equilibrium $CaMnO_3$-(1) modification, and in addition two other hypothetical modifications which were found in two subgroups of *Imma* (space groups *C*2/*m*; Fig. 3*b*, and *C*2/*c*, Fig. 3*c*) and can easily convert to this possible metastable phase. Although the $CaMnO_3$-(5) modification in the space group *Cmcm* appears as a good structural candidate from the group–subgroup relation graph and the GII criterion (Table 1 and Fig. 1), it is known from scanning the literature that this type of distortion is very rare in the perovskite structure family. Furthermore, from the calculated total energies we can see that this *Cmcm* ($CaMnO_3$-(5)) modification has an energy almost identical to one of the experimentally observed modification at the B3LYP level and there appears to be no energy barrier between them. Additionally, $CaMnO_3$-(5) is energetically unfavorable at the LDA level and unstable at the HF level.

In Table 3 we also present the energy difference, $\Delta E$ (in Kelvin), between the various calculated modifications and equilibrium $CaMnO_3$-(1) modification, on the B3LYP level of theory. We suggest that energy differences up to $\sim$ 1800 K are close enough to the experimentally observed modification $CaMnO_3$-(1), and that the corresponding modifications would be possible to observe as a metastable structures at high temperatures (*cf.* Table 2). In contrast, modifications for which the energy difference is higher than $\sim$ 3300 K (Table S3) are unlikely to be experimentally accessible even at high temperatures. Since $CaMnO_3$ melts at temperatures $\sim$ 1773 K (Majewski *et al.*, 2000), the chosen cut-off value of $\sim$ 1800 K appears to be a reasonable one.

For the most important structures, the enthalpy *versus* pressure ($H(p)$) curves were computed at the B3LYP level, in

**Table 2 (continued)**

| Modification, space group and Wyckoff position | Cell parameters (Å), unit-cell volume (Å$^3$) and fractional coordinates | | |
|---|---|---|---|
| | LDA | b3lyp | HF |
| $CaMnO_3$-(15) | $a$ = 2.93, $b$ = 9.53, $c$ = 6.93 | $a$ = 2.97, $b$ = 9.93, $c$ = 7.04 | $a$ = 3.08, $b$ = 10.55, $c$ = 6.79 |
| *Cmcm* (63) | $V$ = 193.20 | $V$ = 207.60 | $V$ = 220.49 |
| Ca 4*c* | 0 0.2491 1/4 | 0 0.2481 1/4 | 0 0.2401 1/4 |
| Mn 4*a* | 0 0 0 | 0 0 0 | 0 0 0 |
| O1 4*c* | 1/2 0.4339 1/4 | 1/2 0.4337 1/4 | 1/2 0.4178 1/4 |
| O2 8*f* | 1/2 0.1230 0.0479 | 1/2 0.1218 0.0514 | 1/2 0.1197 0.0800 |
| $CaMnO_3$-(16) | $a$ = 5.13, $c$ = 14.34 | $a$ = 5.22, $c$ = 14.88 | $a$ = 5.37, $c$ = 14.95 |
| $R\bar{3}$ (148) | $V$ = 326.48 | $V$ = 351.08 | $V$ = 373.56 |
| Ca 6*c* | 0 0 0.8671 | 0 0 0.8642 | 0 0 0.8606 |
| Mn 6*c* | 0 0 0.6589 | 0 0 0.6509 | 0 0 0.6468 |
| O 18*f* | 0.2752 −0.0727 0.4051 | 0.2806 −0.0609 0.4048 | 0.2918 −0.0509 0.4055 |

† At the Hartree–Fock (HF) level of theory the corresponding structure was unstable.

**Table 3**
Energies in hartrees ($E_h$) per formula unit (at a pressure of 0 GPa) of the energetically most favorable structures at calculated equilibrium volumes.

The local optimizations were performed within HF, B3LYP (sorted by energy ascending) and LDA approximation. Energy difference between modifications on B3LYP level of theory is given in Kelvin.

| | Method | | | |
|---|---|---|---|---|
| Modification | LDA | b3lyp | HF | $\Delta E$ (B3LYP) (K) |
| $CaMnO_3$-(1) | −2048.9104 | −2054.2589 | −2051.1170 | 0 |
| $CaMnO_3$-(5) | −2048.9020 | −2054.2583 | † | ∼ 190 |
| $CaMnO_3$-(10) | −2048.9057 | −2054.2582 | −2051.1374 | ∼ 220 |
| $CaMnO_3$-(3) | −2048.9002 | −2054.2576 | −2051.1172 | ∼ 410 |
| $CaMnO_3$-(13) | −2048.9018 | −2054.2553 | † | ∼ 1140 |
| $CaMnO_3$-(15) | −2048.8912 | −2054.2549 | −2051.0964 | ∼ 1260 |
| $CaMnO_3$-(4) | −2048.9071 | −2054.2545 | † | ∼ 1390 |
| $CaMnO_3$-(12) | −2048.9001 | −2054.2538 | −2051.1376 | ∼ 1600 |
| $CaMnO_3$-(9) | −2048.9005 | −2054.2532 | −2051.0867 | ∼ 1800 |
| $CaMnO_3$-(2) | −2048.9124 | −2054.2483 | −2051.0822 | ∼ 3300 |
| $CaMnO_3$-(14) | −2048.9120 | −2054.2479 | −2051.0845 | ∼ 3500 |
| $CaMnO_3$-(8) | −2048.9014 | −2054.2470 | −2051.0832 | ∼ 3800 |
| $CaMnO_3$-(6) | −2048.9004 | −2054.2463 | −2051.0569 | ∼ 4000 |
| $CaMnO_3$-(7) | −2048.8993 | −2054.2425 | −2050.9875 | ∼ 5200 |
| $CaMnO_3$-(11) | −2048.8961 | −2054.2318 | −2050.8024 | ∼ 8550 |
| $CaMnO_3$-(16) | −2048.8818 | −2054.2387 | −2051.0691 | ∼ 6400 |

† At the Hartree–Fock (HF) level of theory the corresponding structure was unstable.

order to investigate the pressure dependence of the $CaMnO_3$ phases (Figs. 5*a* and *b*). As expected each of the perovskite-like phases generated with SPuDS and data mining were metastable at standard pressure compared with the equilibrium $CaMnO_3$-(1) structure. This is also in agreement with the GII criterion (see Table 1).

However, as we have shown above, additional $ABX_3$ non-perovskite phases may be competitive with $CaMnO_3$-(1) if we vary the pressure. Thus, using the hybrid B3LYP functional, we predict a pressure-induced phase transition at 35 GPa, going from the perovskite-related $CaMnO_3$-(1) (*Pnma*) structure to the layered post-perovskite structure $CaMnO_3$-(15) (space group *Cmcm*; Fig. 6*a*). This post-perovskite phase was observed for the first time in $CaIrO_3$; there has been no experimental or theoretical evidence of this phase in $CaMnO_3$ up to now.

In addition there is a transition in the effective negative pressure region, between the $CaMnO_3$-(1) perovskite structure and the $CaMnO_3$-(16) modification in the ilmenite structure type at around −3 GPa, calculated at the B3LYP level of theory (Figs. 5*b* and 6*b*). Such perovskite → ilmenite phase transitions have been observed experimentally and theoretically in various compounds (Nancy & McMillan, 1984; Sesion *et al.*, 2010); however, to our knowledge, no experimental or calculated data exist regarding a possible ilmenite structure type in the $CaMnO_3$ system.

## 4. Discussion

Beyond the energetic considerations regarding the thermodynamic stability of the proposed modifications, we have analyzed interatomic distances and angles for the experimentally observed *Pnma* structure and compare it to our calculated models (Table 4). We note that the anisotropy of the unit cell fit the best to the LDA results. On the other hand, we can see that the results for average Mn—O and Ca—O distances, as well as for the bond angles obtained using the B3LYP functional are in the best agreement with experimentally observed results (Božin *et al.*, 2008). In addition, total energies, cell parameters and unit-cell volume favors the B3LYP method compared with other *ab initio* methods (Fig. 4 and Table 3 and Table S2), and thus only the B3LYP results will be considered for further structure analysis.

In the next step we analyzed the interatomic distances for each of the investigated modifications calculated using the B3LYP functional (Table S4), and the distribution of the average value for Mn—O and Ca—O distances. Furthermore, we have investigated the value of the Ca—Mn shortest distance, since in some cases it can be used as a criterion for the determination of the *A*-site cation coordination (Mitchell, 2002). We find that the average value of the Mn—O distance is in the range 1.90–1.91 Å for most of the distortions considered. The average value of the Ca—O distances lie between 2.5 and 2.6 Å. We note that this number can slightly differ depending on which Ca atom is chosen for the central atom (see Table S4). The shortest Ca—Mn bond has the value 3.11 Å in the orthorhombic $CaMnO_3$-(1) modification, and rises to 3.24 Å for the cubic $CaMnO_3$-(11) modification. The table also contains information about the volumes of the polyhedra around Ca and Mn.

Finally, we have analyzed the Mn—O—Mn angles in the various $CaMnO_3$ perovskite-type configurations since this analysis can give us more insight in the tilting and the

**Table 4**
Comparison between experimentally determined and calculated interatomic distances (Å) and angles (°) in orthorhombic *Pnma*.

| Method | Mn—O | ⟨Mn—O⟩ | ⟨Ca—O⟩ | Mn—O1—Mn | Mn—O2—Mn |
|---|---|---|---|---|---|
| Experiment (Božin *et al.*, 2008) | 2 × 1.8953 (1) (O1)<br>2 × 1.8972 (6) (O2)<br>2 × 1.9053 (6) (O2) | 1.8993 | 2.6520 (XII) | 158.15 (8) | 156.90 (8) |
| LDA | 2 × 1.8612 (O1)<br>2 × 1.8548 (O2)<br>2 × 1.8576 (O2) | 1.8578 | 2.5971 (XII) | 160.50 | 157.62 |
| B3LYP | 2 × 1.8528 (O1)<br>2 × 1.8989 (O2)<br>2 × 1.9660 (O2) | 1.9059 | 2.6646 (XII) | 160.24 | 157.45 |
| HF | 2 × 2.0884 (O1)<br>2 × 1.9545 (O2)<br>2 × 1.9603 (O2) | 2.0011 | 2.7663 (XII) | 141.85 | 155.22 |

distortion of the ideal perovskite structure. For example, the ideal cubic $Pm\bar{3}m$ perovskite has only one type of bond with a perfect 180° angle between them, while the equilibrium *Pnma* structure shows two types of bonds, depending on the choice of oxygen, with angles Mn—O1—Mn = 160.24° and Mn—O2—Mn = 157.45°. These changes in angles directly correspond to the structural changes caused by the tilting of the octahedra.

Phase transitions appear quite frequently in perovskite-type compounds and the presence/magnitude of octahedral tilting greatly influences the physical properties of the material. $CaMnO_3$ is the parent compound for many rare-earth doped manganese perovskite oxides that exhibit colossal magneto-resistance (Jin *et al.*, 1994). Therefore, it is important to understand the changes in the structure of $CaMnO_3$ as a function of pressure and temperature. To investigate these issues, we have applied different theoretical methods to explore the possible modifications of this chemical system, where up to now only the experimentally observed orthorhombic modification is known to exist.

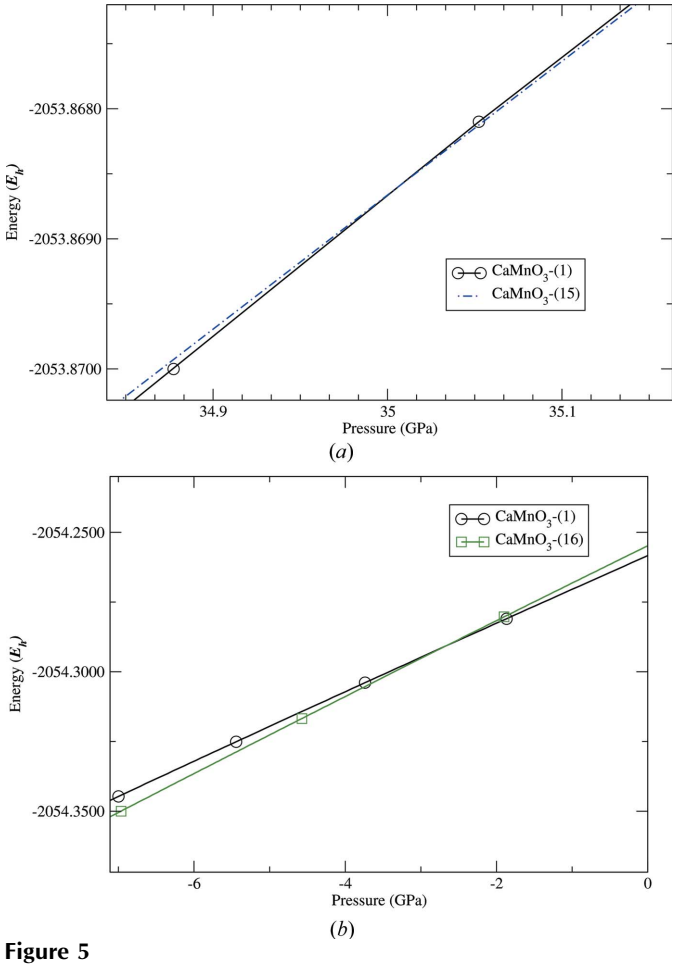


**Figure 5**
$H(p)$ curves at the B3LYP level of calculation for the most relevant modifications of $CaMnO_3$ participating in pressure-induced phase transitions: (*a*) at elevated pressures perovskite [$CaMnO_3$-(1)] structure transforms to the post-perovskite [$CaMnO_3$-(15)] phase; (*b*) at effective negative pressures perovskite [$CaMnO_3$-(1)] structure transforms to the ilmenite [$CaMnO_3$-(16)] phase. Enthalpies per one formula unit are given in hartrees ($E_h$).

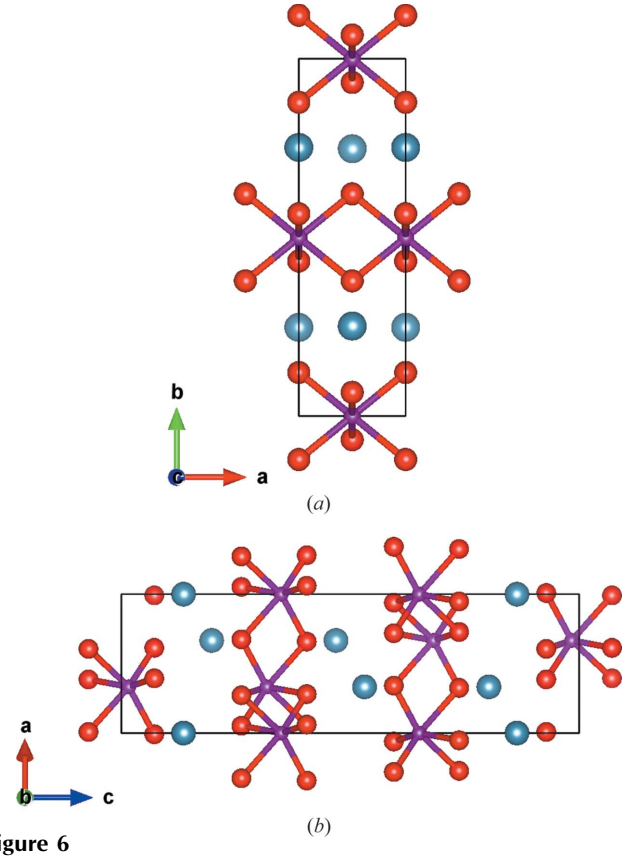


**Figure 6**
Calculated $CaMnO_3$ modifications using the B3LYP approximation: (*a*) a post-perovskite $CaMnO_3$-(15) phase in the space group *Cmcm* and (*b*) $CaMnO_3$-(16) in space group $R\bar{3}$ with the ilmenite structure type. Mn (violet) and O (red) atoms are bonded, while Ca atoms are colored blue. The unit cell is marked with a quadrangle.

Considering Fig. 4 we note that all the low-energy structures $CaMnO_3$-(3, 4, 5, 9, 10, 12, 13) are within $k_BT_{melt}$ of the lowest energy phase, and $CaMnO_3$-(3, 5, 10) are within $k_BT$ even at room temperature, and are thus expected to become competitive at elevated temperatures (Table 3). Therefore, disregarding the issue of kinetic stability, we can conclude that the metastable modifications which are close to the thermodynamical equilibrium phase $CaMnO_3$-(1) are expected to be easier to synthesize, *e.g.* at elevated temperatures or for slight degrees of chemical disorder, than those like $CaMnO_3$-(2, 6, 7, 8, 11, 14) which are close to the energetically most unfavorable cubic aristotype. However, we note that the perovskite cubic phase is known to occur in many $ABX_3$ compounds as the ideal high-temperature form.

In this context we mention that there have been claims in the literature that a cubic phase of $CaMnO_3$ at high temperatures has been observed, as well as several other structures as intermediate phases along high-temperature phase transitions of usually non-stoichiometric $CaMnO_3$ (Poeppelmeier *et al.*, 1982; Taguchi *et al.*, 1989; Rørmark *et al.*, 2002). For example, Taguchi *et al.* performed an experiment on non-stoichiometric $CaMnO_{3-\delta}$ and they observed a phase transition away from the orthorhombic phase at 1169 K to a tetragonal modification ($a$ = 5.333, $c$ = 7.534 Å), which could resemble our $CaMnO_3$-(7) modification. With a further increase of temperature a second phase transition occurred from this intermediary tetragonal to the cubic phase at 1186 K ($a$ = 3.774 Å), which again coincides with our $CaMnO_3$-(11) modification and calculated $E(V)$ curves. So far, this high-temperature behavior has only been found for the non-stoichiometric modification, where the oxygen deficiency clearly affects the structural and physical properties. Additional complexity in the non-stoichiometric system comes from the fact that $Mn^{4+}$ is reduced to $Mn^{3+}$, which introduces the Jahn–Teller effect and the distortion of coordination polyhedra[5] (Mitchell, 2002). However, if this cubic metastable structure could also be reached in the stoichiometric $CaMnO_3$ compound, then several of the generally rather unlikely $CaMnO_3$ modifications listed in Table S3 may be observable as part of the cubic perovskite basin on the energy landscape for similar synthesis conditions. Furthermore, our recent experimental results (Bošković *et al.*, 2008; Zagorac *et al.*, 2014) show that properties of $CaMnO_3$ nanopowders can be affected by doping. In that respect, the newly developed CCL algorithm implemented in the KPLOT program (Hundt *et al.*, 2013) could help investigate nanosized structures.

We note that perovskite structures in space groups $P2_1/m$ and $P\overline{1}$ are low in symmetry and computationally very expensive, and we have not considered these structure models in this study. In principle, it is possible to perform exhaustive global and local searches which should bring additional structure candidates, *e.g.* simulated annealing (Kirkpatrick *et al.*, 1983), exhaustive data mining (Sultania *et al.*, 2012), prescribed path calculations (Zagorac, Schön & Jansen, 2012) or threshold algorithm calculations (Schön *et al.*, 1996); or focus on the properties of each of the separately calculated structures (Zagorac, Doll, Schön & Jansen, 2012). However, these methods are computationally expensive and demand a separate study, which could be the focus of the future work.

Finally, the post-perovskite ($CaIrO_3$-type) and ilmenite-type modifications represent alternative $CaMnO_3$ modifications belonging to energy landscape regions remote from that containing the perovskite modifications, since they exhibit very different structure types. Thus, they have not been included in the discussion about the geometrical differences and similarities among the perovskite family modifications. However, both the $CaIrO_3$ type and the ilmenite-type modifications are highly relevant if one considers pressure-driven phase transformations. As the $CaMnO_3$-(15) structure type also occurs in other $ABX_3$ systems (usually at high pressures (Oganov *et al.*, 2005), we would like to propose this modification as a good candidate for high-pressure synthesis.

## 5. Conclusion

We have performed crystal structure prediction in the $CaMnO_3$ system, focusing on modifications related to the perovskite type of structure. Using systematic octahedral tilting in the ideal cubic perovskite structure and data mining in structurally related $ABX_3$ systems, a set of $CaMnO_3$ structure candidates was generated. For every candidate, local optimizations on the *ab initio* level using density functional theory (LDA, and hybrid B3LYP functionals) and Hartree–Fock (HF) were performed, where the results obtained using the B3LYP functional showed the best agreement with existing experimental data belonging to the known orthorhombic (*Pnma*) modification of $CaMnO_3$. Our results suggest that several of the low-energy structure candidates, mostly with orthorhombic or monoclinic symmetry, which exhibit some structural similarity with the experimentally known structure, may be synthetically accessible at elevated temperatures and/or for slightly non-stoichiometric compositions.

In contrast, the modifications similar to the ideal perovskite (in the $Pm\overline{3}m$ space group) are only expected to exist in non-stoichiometric $CaMnO_3$ compounds. Upon varying the pressure we predict a post-perovskite modification exhibiting the $CaIrO_3$ structure type to be thermodynamically stable at pressures above 35 GPa. Similar calculations at effective negative pressures show a second pressure-driven phase transition from the perovskite to the ilmenite structure type at *ca* −3 GPa. Thus, this study yields new insight into the $CaMnO_3$ system at high and effective negative pressures, and reveals relationships between possible metastable perovskite family phases.

## 6. Related literature

References cited in the supporting information include: Boukhalov & Solovyev (2010), Božin *et al.* (2008), Caracas & Wentzcovitch (2006), Damay *et al.* (1998), Darlington &

[5] We note that in the calculated stoichiometric $CaMnO_3$ compound there is no Jahn–Teller effect, due to the absence of $Mn^{3+}$.

Knight (1999), Kennedy *et al.* (2009), Moussa *et al.* (2001), Panunzio Miner *et al.* (2007), Shirako *et al.* (2009), Trang *et al.* (2011), Yamanaka (2005), Yanchevskii *et al.* (2008), Weitin *et al.* (2009).

The authors would like to thank R. Hundt for valuable discussions. This paper has been financially supported by the Ministry of Science of the Republic of Serbia, as part of project No. III45012.

## References


Aleksandrov, K. S. (1976). *Kristallografiya*, **21**, 249–255.

Avdeev, M., Caspi, E. N. & Yakovlev, S. (2007). *Acta Cryst.* B**63**, 363–372.

Bergerhoff, G. & Brown, I. D. (1987). *Crystallographic Databases*, edited by F. H. Allen, G. Bergerhoff & R. Sievers. Chester: International Union of Crystallography.

Bhattacharjee, S., Bousquet, E. & Ghosez, P. (2009). *Phys. Rev. Lett.* **102**, 117602.

Bošković, S., Dukić, J., Matović, B., Živković, L., Vlajić, M. & Krstić, V. (2008). *J. Alloys Compd.* **463**, 282–287.

Boukhalov, D. W. & Solovyev, I. V. (2010). *Phys. Rev. B*, **82**, 245101.

Božin, E. S., Sartbaeva, A., Zheng, H., Wells, S. A., Mitchell, J. F., Proffen, T., Thorpe, M. F. & Billinge, S. J. L. (2008). *J. Phys. Chem. Solids*, **69**, 2146–2150.

Brown, I. D. (1992). *Acta Cryst.* B**48**, 553–572.

Brown, I. D. (2002). *The Chemical Bond in Inorganic Chemistry.* Oxford University Press.

Brown, I. D. & Altermatt, D. (1985). *Acta Cryst.* B**41**, 244–247.

Caracas, R. & Wentzcovitch, R. M. (2006). *Acta Cryst.* B**62**, 1025–1030.

Coey, J. M. D., Viret, M. & von Molnár, S. (1999). *Adv. Phys.* **48**, 167–293.

Colla, E. L., Reaney, I. M. & Setter, N. (1993). *J. Appl. Phys.* **74**, 3414–3425.

Damay, F., Jirak, Z., Hervieu, M., Martin, C., Maignan, A., Raveau, B., Andre, G. & Bouree, F. (1998). *J. Magn. Magn. Mater.* **190**, 221–232.

Darlington, C. N. W. & Knight, K. S. (1999). *Acta Cryst.* B**55,** 24–30.

Doll, K., Saunders, V. R. & Harrison, N. M. (2001). *Int. J. Quantum Chem.* **82**, 1–13.

Dovesi, R., Orlando, R., Civalleri, B., Roetti, C., Saunders, V. R. & Zicovich-Wilson, C. M. (2005). *Z. Kristallogr.* **220**, 571–573.

Ederer, C. & Spaldin, N. A. (2006). *Phys. Rev. B*, **74**, 0241028.

Evarestov, R. A., Blokhin, E., Gryaznov, D., Kotomin, E. A. & Maier, J. (2011). *Phys. Rev. B*, **83**, 134108.

Freyria Fava, F. F., D'Arco, P., Orlando, R. & Dovesi, R. (1997). *J. Phys. Condens. Matter*, **9**, 489–498.

García-Fernández, P., Ghosh, S., English, N. J. & Aramburu, J. A. (2012). *Phys. Rev. B*, **86**, 144107.

Glazer, A. M. (1972). *Acta Cryst.* B**28**, 3384–3392.

Goldschmidt, V. M. (1926). *Skrifter Norske Videnskaps-Akad. Mater. Naturvid. Kl.* No. 2.

Hannemann, A., Hundt, R., Schön, J. C. & Jansen, M. (1998). *J. Appl. Cryst.* **31**, 922–928.

Howard, C. J. & Stokes, H. T. (1998). *Acta Cryst.* B**54**, 782–789.

Hundt, R. (2012). *KPLOT.* University of Bonn, Germany.

Hundt, R., Schön, J. C., Hannemann, A. & Jansen, M. (1999). *J. Appl. Cryst.* **32**, 413–416.

Hundt, R., Schön, J. C., Neelamraju, S., Zagorac, J. & Jansen, M. (2013). *J. Appl. Cryst.* **46**, 587–593.

Hwang, H. Y., Palstra, T. T. M., Cheong, S. W. & Batlogg, B. (1995). *Phys. Rev. B*, **52**, 15046–15049.

Jin, S., Tiefel, T. H., McCormack, M., Fastnacht, R. A., Ramesh, R. & Chen, L. H. (1994). *Science*, **264**, 413–415.

Kennedy, B. J., Saines, P. J., Ting, J., Zhou, Q. & Kimpton, J. A. (2009). *J. Solid State Chem.* **182**, 2858–2866.

Kirkpatrick, S., Gelatt, C. D. & Vecchi, M. P. (1983). *Science*, **220**, 671–680.

Locherer, T., Dinnebier, R., Kremer, R., Greenblatt, M. & Jansen, M. (2012). *J. Solid State Chem.* **190**, 277–284.

Lufaso, M. W. & Woodward, P. M. (2001). *Acta Cryst.* B**57**, 725–738.

Lufaso, M. W. & Woodward, P. M. (2004). *Acta Cryst.* B**60**, 10–20.

Magyari-Köpe, B., Vitos, L., Johansson, B. & Kollár, J. (2001). *Acta Cryst.* B**57**, 491–496.

Maier, B. J., Waeselmann, N., Mihailova, B., Angel, R. J., Ederer, C., Paulmann, C., Gospodinov, M., Friedrich, A. & Bismayer, U. (2011). *Phys. Rev. B*, **84**, 174104.

Majewski, P., Epple, L., Rozumek, M., Schluckwerder, H. & Aldinger, F. (2000). *J. Mater. Res.* **15**, 1161–1166.

Mitchell, R. H. (2002). *Perovskites: Modern and Ancient.* Thunder Bay: Almaz Press.

Mitchell, R. H. & Liferovich, R. P. (2005). *J. Solid State Chem.* **178**, 2586–2593.

Momma, K. & Izumi, F. (2011). *J. Appl. Cryst.* **44**, 1272–1276.

Moussa, S. M., Kennedy, B. J. & Vogt, T. (2001). *Solid State Commun.* **119**, 549–552.

Nancy, L. R. & McMillan, P. (1984). *Am. Mineral.* **69**, 719–721.

Panunzio Miner, E. V., De Paoli, J. M., Alonso, J. A., Garcia-Heernandez, M., Sanchez, R. D. & Carbonio, R. E. (2007). *Physica B*, **398**, 397–400.

Oganov, A. R., Martonák, R., Laio, A., Raiteri, P. & Parrinello, M. (2005). *Nature*, **438**, 1142–1144.

Paszkowicz, W., Woodley, S. M., Piszora, P., Bojanowski, B., Piętosa, J., Cerenius, Y., Carlson, S. & Martin, C. (2013). *Appl. Phys. A*, **112**, 839–845.

Piskunov, S., Heifets, E., Eglitis, R. & Borstel, G. (2004). *Comput. Mater. Sci.* **29**, 165–178.

Poeppelmeier, K. R., Leonowicz, M. E., Scanlon, J. C. & Longo, J. M. (1982). *J. Solid State Chem.* **45**, 71–79.

Raveau, B., Maignan, A., Martin, C. & Hervieu, M. (1998). *Chem. Mater.* **10**, 2641–2652.

Rørmark, L., Wiik, K., Stølen, S. & Grande, T. (2002). *J. Mater. Chem.* **12**, 1058–1067.

Salinas-Sanchez, A., Garcia-Muñoz, J. L., Rodriguez-Carvajal, J., Saez-Puche, R. & Martinez, J. (1992). *J. Solid State Chem.* **100**, 201–211.

Schön, J. C., Cancarević, Z. & Jansen, M. (2004). *J. Chem. Phys.* **121**, 2289–2304.

Schön, J. C., Putz, H. & Jansen, M. (1996). *J. Phys. Condens. Matter*, **8**, 143–156.

Sesion, P. D., Henriques, J. M., Barboza, C. A., Albuquerque, E. L., Freire, V. N. & Caetano, E. W. (2010). *J. Phys. Condens. Matter*, **22**, 435801.

Shirako, Y., Kojitani, H., Akaogi, M., Yamaura, K. & Takayama-Muromachi, E. (2009). *Phys. Chem. Miner.* **36**, 455–462.

Sultania, M., Schön, J. C., Fischer, D. & Jansen, M. (2012). *Struct. Chem.* **23**, 1121–1129.

Taguchi, H. (1996). *J. Solid State Chem.* **124**, 360–365.

Taguchi, H., Nagao, M., Sato, T. & Shimada, M. (1989). *J. Solid State Chem.* **78**, 312–315.

Thomas, N. W. (1996). *Acta Cryst.* B**52**, 16–31.

Thomas, N. W. (1998). *Acta Cryst.* B**54**, 585–599.

Tong, J., Lee, C., Whangbo, M.-H., Kremer, R. K., Simon, A. & Köhler, J. (2010). *Solid State Sci.* **12**, 680–684.

Trang, N. T., Cong, B. T., Thao, P. H., Tan, P. T., Tho, N. D. & Nhat, H. N. (2011). *Physica B*, **406**, 3613–3621.

Vecherskii, S. I., Konopel'ko, M. A., Esina, N. O. & Batalov, N. N. (2002). *Inorg. Mater.* **38**, 1270–1276.

Weitin, C., Williams, A. J., San Martin, L. O., Li, M., Sinclair, D. C., Zhou, W. & Attfield, P. (2009). *Chem. Mater.* **21**, 2085–2093.

Wentzcovitch, R. M., Ross, N. L. & Price, G. (1995). *Phys. Earth Planet. Inter.* **90**, 101–112.
Woodward, P. M. (1997). *Acta Cryst.* B**53**, 32–43.
Yamanaka, T. (2005). *J. Synchrotron Rad.* **12**, 566–576.
Yanchevskii, O. Z., Tovstolytkin, A. I., V'yunov, O. I. & Belous, A. G. (2008). *Inorg. Mater.* **44**, 181–188.
Zagorac, J., Boskovic, S., Matovic, B. & Babic Stojic, B. (2010). *Sci. Sint.* **42**, 221–232.
Zagorac, D., Doll, K., Schön, J. C. & Jansen, M. (2011). *Phys. Rev. B*, **84**, 045206.
Zagorac, D., Doll, K., Schön, J. C. & Jansen, M. (2012). *Chem. Eur. J.* **18**, 10929–10936.
Zagorac, D., Schön, J. C. & Jansen, M. (2012). *J. Phys. Chem. C*, **116**, 16726–16739.
Zagorac, D., Schön, J. C., Zagorac, J. & Jansen, M. (2014). *Phys. Rev. B*, **89**, 075201.
Zagorac, D., Schön, C., Zagorac, J., Pentin, I. V. & Jansen, M. (2013). *Process. Appl. Ceram.* **7**, 111–116.
Zagorac, J., Zarubica, A., Radosavljevic Mihajlovic, A., Zagorac, D. & Matovic, B. (2014). *Bull. Mater. Sci.* **37**, 1–10.
Zhao, J., Ross, N. L. & Angel, R. J. (2004). *Acta Cryst.* B**60**, 263–271.
Zhou, Q. & Kennedy, B. J. (2006). *J. Phys. Chem. Solids*, **67**, 1595–1598.